The Mcm2-Ctf4-Polα Axis Facilitates Parental Histone H3-H4 Transfer to Lagging Strands

Gan, Haiyun; Serra-Cardona, Albert; Hua, Xu; Zhou, Hui; Labib, Karim; Yu, Chuanhe

Published in:
Molecular Cell

DOI:
10.1016/j.molcel.2018.09.001

Publication date:
2018

Supplementary Materials for

The Mcm2-Ctf4-Polα axis facilitates parental histone H3-H4 transfer to lagging strands

Haiyun Gan[1*], Albert Serra-Cardona[1*], Xu Hua[1], Hui Zhou[1], Karim Labib[2], Chuanhe Yu[3†] and Zhiguo Zhang[1†‡]

* These authors contributed equally to this work

† Corresponding authors: Zhiguo Zhang (zz2401@cumc.columbia.edu), Chuanhe Yu (yu.chuanhe@mayo.edu)

‡Lead contact: Zhiguo Zhang (zz2401@cumc.columbia.edu)

List of Supplementary Materials:

Figure S1. Related to Figure 1; **Figure S2**. Related to Figure 2; **Figure S3**. Related to Figure 4; **Figure S4**. Related to Figure 5; **Figure S5**. Related to Figure 6; **Figure S6**. Related to Figure 6.

Tables S1 - S2

Figure S1

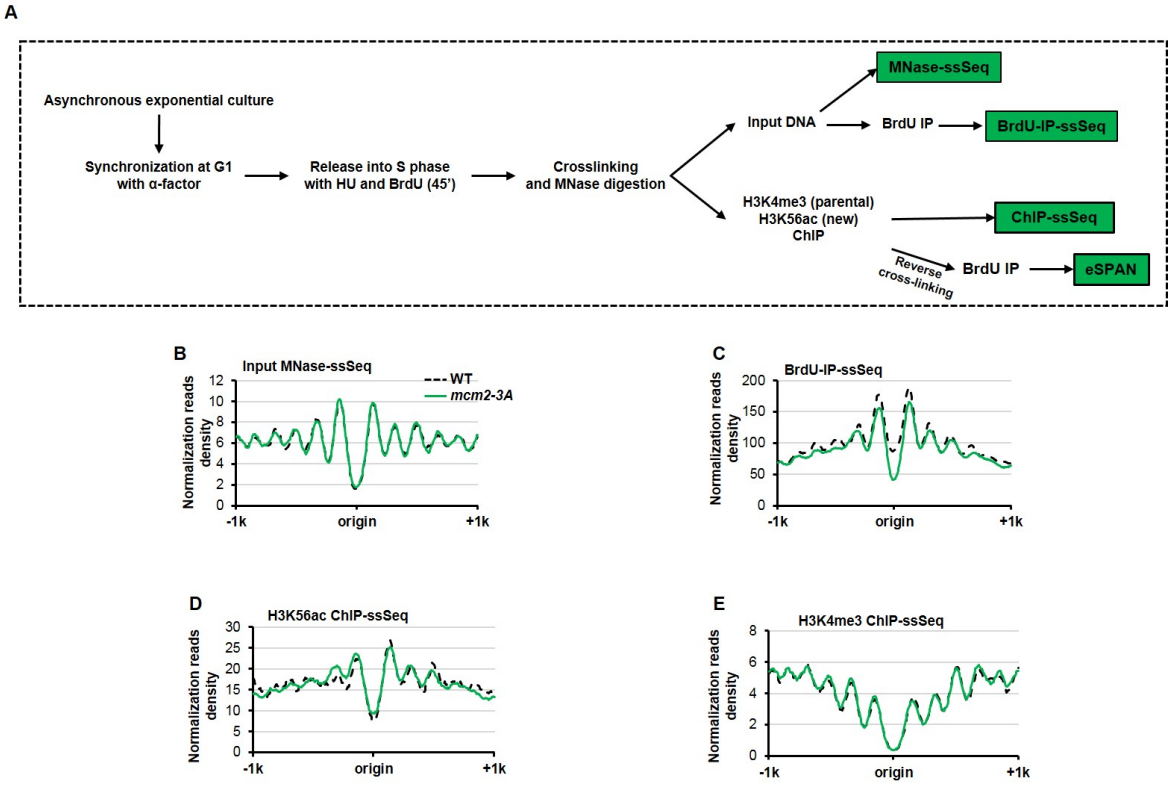

Figure S1. The *mcm2-3A* mutation has no apparent effect on overall nucleosome occupancy and positioning surrounding early DNA replication origins. Related to Figure 1. (A) Schematic outline of the experimental procedures for MNase-ssSeq, BrdU-IP-ssSeq, ChIP-ssSeq and eSPAN. **(B-E)** Average nucleosome profiles of MNase-ssSeq of input samples (B), BrdU-IP-ssSeq (C), H3K56ac ChIP-ssSeq (D), and H3K4me3 ChIP-ssSeq (E) surrounding 134 early replication origins in wild type and *mcm2-3A* cells. Total sequence reads with the size from 120-170 bp fragments were selected to determine the average nucleosome density of the region surrounding the 134 early replication origins. Nucleosome occupancy within 1 kb from each early replication origin was shown.

Figure S2

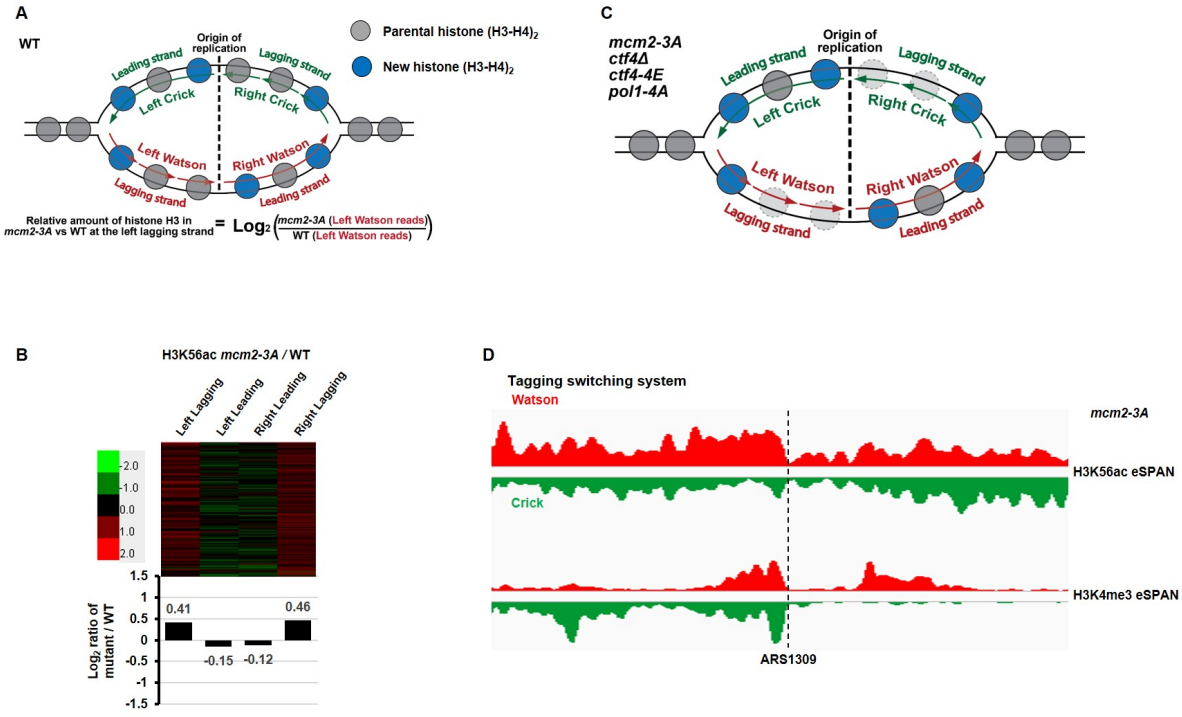

Figure S2. H3K4me3 and H3K56ac eSPAN peaks in *mcm2-3A* mutant cells display a leading and lagging strand bias pattern, respectively, in the Recombination-Induced Tag Exchange (RITE) strain. Related to Figure 2. (A) Model representing the distribution of parental and new $(H3\text{-}H4)_2$ tetramers at DNA replication forks. In WT cells, parental histones (H3K4me3) show a slight preference for the lagging strand (Yu et al., 2018). Lower panel: equation for calculating the relative amount of histone H3 at the left lagging strand in *mcm2-3A* vs WT. **(B)** The *mcm2-3A* mutation has a minor impact on the relative amount of H3K56ac compared to wild type. Top: heatmap representing the relative level of H3K56ac in *mcm2-3A* mutant cells compared to wild type cells at each of the 134 individual origins (0: no difference between mutant and wild type (black); <0 and >0 represent less (green) and more (red) H3K56ac eSPAN sequence reads in *mcm2-3A* cells than in wild type cells, respectively). Bottom: the average of relative amount of H3K56ac at lagging and leading strands of 134 replication origins in *mcm2-3A* cells compared to wild type cells. **(C)** A model explaining the impairment of the

transfer of parental $(H3\text{-}H4)_2$ to lagging strands in *mcm2-3a*, *ctf4*Δ, *ctf4-4E* and *pol1-4A* cells compared to WT model shown in Figure S2A, which leads to differences in H3K4me3 and H3K56ac eSPAN bias patterns between WT and mutant cells. **(D)** Snapshot of H3K4me3 and H3K56ac eSPAN peaks at individual nucleosomes surrounding *ARS1309* in *mcm2-3A* mutant cells, which is from the same experiment as Figure 2.

Figure S3

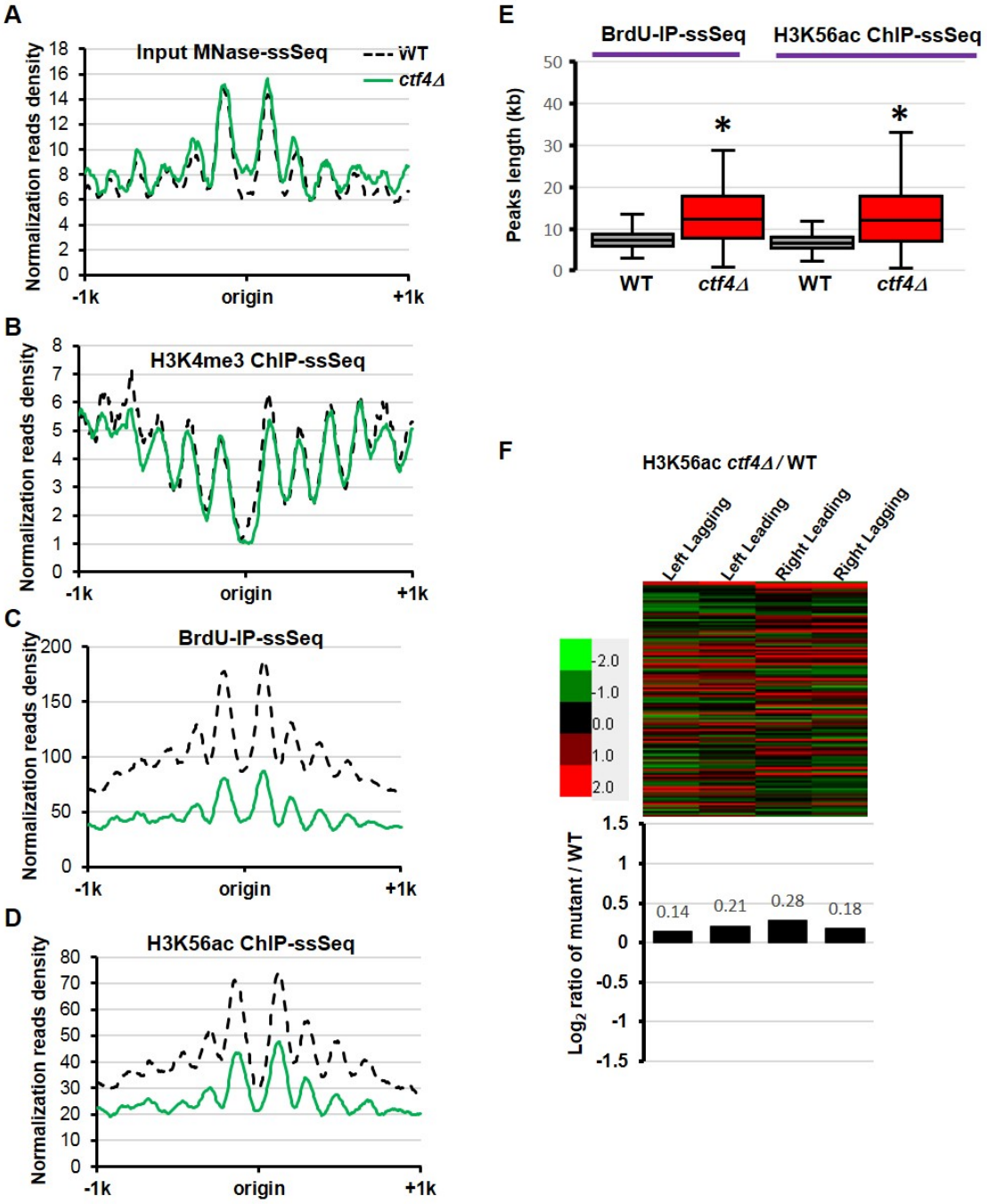

Figure S3. Deletion of *CTF4* has little impact on nucleosome occupancy at replicating chromatin as detected by MNase-ssSeq and H3K4me3 ChIP-ssSeq compared to wild type cells. Related to Figure 4. (A-D) Average nucleosome profiles of MNase-ssSeq of input samples (A), H3K4me3 ChIP-ssSeq (B), BrdU-IP-ssSeq (C), and H3K56ac ChIP-ssSeq (D) surrounding 134 early replication origins in wild type and

ctf4Δ cells. Nucleosome density was calculated following the same procedure as in Figure S1. As explained in the main text, the reduced nucleosome occupancy as detected by H3K56ac ChIP-ssSeq and BrdU-IP-ssSeq is likely due to normalization effect as DNA synthesis in *ctf4*Δ cells proceeds longer than wild type cells (Figure S3E). (**E**) DNA synthesis in *ctf4*Δ cells proceeds further than in wild type cells. Box plot showing the distribution of BrdU-IP-ssSeq and H3K56ac ChIP-ssSeq peak length at 134 early replication origins in WT and *ctf4*Δ cells. The H3K56ac ChIP-ssSeq and BrdU-IP-ssSeq peaks were identified by SICER software with a false discovery rate (FDR) cut-off of 0.01. Asterisks indicate $p < 0.01$ (two-tailed Student's t test). As discussed in the main text, this elongated DNA synthesis is probably due to increased dNTP concentrations detected in *ctf4*Δ cells. **(F)** Deletion of *CTF4* has a minimal impact on the relative amount of H3K56ac at both leading and lagging strands compared to wild type cells. Top: heatmap representing the relative level of H3K56ac in *ctf4Δ* mutant cells compared to wild type cells at each of the 134 individual origins (0: no difference between mutant and wild type (black); <0 and >0 represent less (green) and more (red) H3K56ac eSPAN sequence reads in *ctf4Δ* cells than in wild type cells, respectively). Bottom: the average of the relative amount of H3K56ac at lagging and leading strands of 134 replication origins in *ctf4Δ* cells compared to wild type cells.

Figure S4

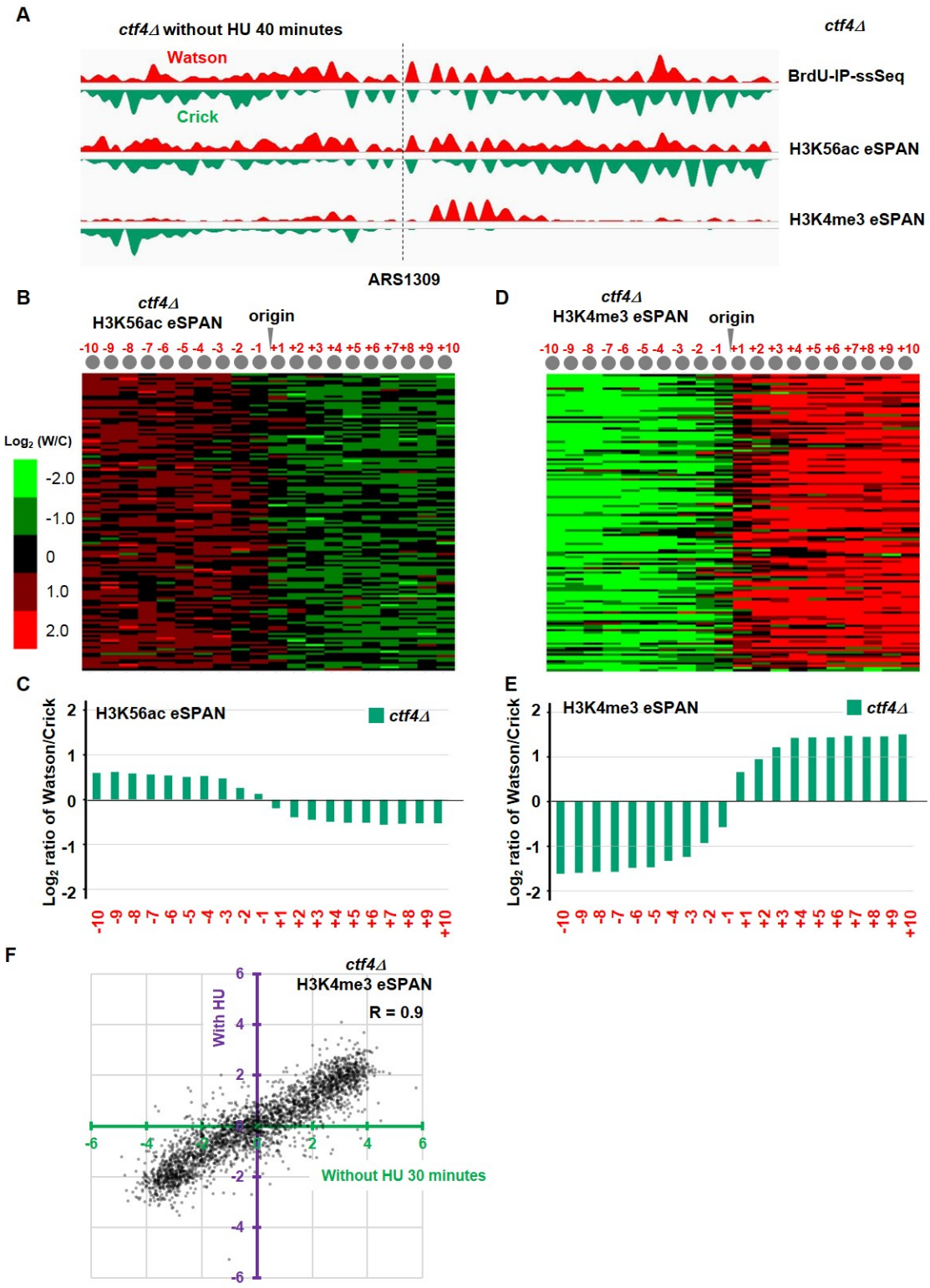

Figure S4. The H3K4me3 eSPAN peaks in *ctf4*Δ mutant cells show a marked leading strand bias under normal cell cycle progression. Related to Figure 5. (A) Snapshot

of BrdU IP-ssSeq, H3K56ac and H3K4me3 eSPAN peaks surrounding the *ARS1309* in *ctf4*Δ mutant cells under normal cell cycle progression. The experiments were performed at the same time as Figure 5 except that samples were collected at 40 minutes after release from G1 cells. **(B-E)** In the absence of HU, the H3K56ac and H3K4me3eSPAN peaks in *ctf4*Δ mutant cells show a strong lagging- and leading-strand bias, respectively. They display the same bias pattern as the ones with HU (Figure 4). H3K56ac and H3K4me3 eSPAN results of *ctf4*Δ mutant cells were presented as Heatmaps (B, D) of the bias pattern at each of 134 replication origins and as bar graph of the average bias pattern of all origins (C and E). **(F)** The dot scatter plots show the H3K4me3 bias pattern in *ctf4Δ* mutant cells with HU vs without HU condition. One dot represents the bias ratio of eSPAN peaks at individual nucleosomes (±10 nucleosomes) surrounding each of 134 early DNA replication origins.

Figure S5

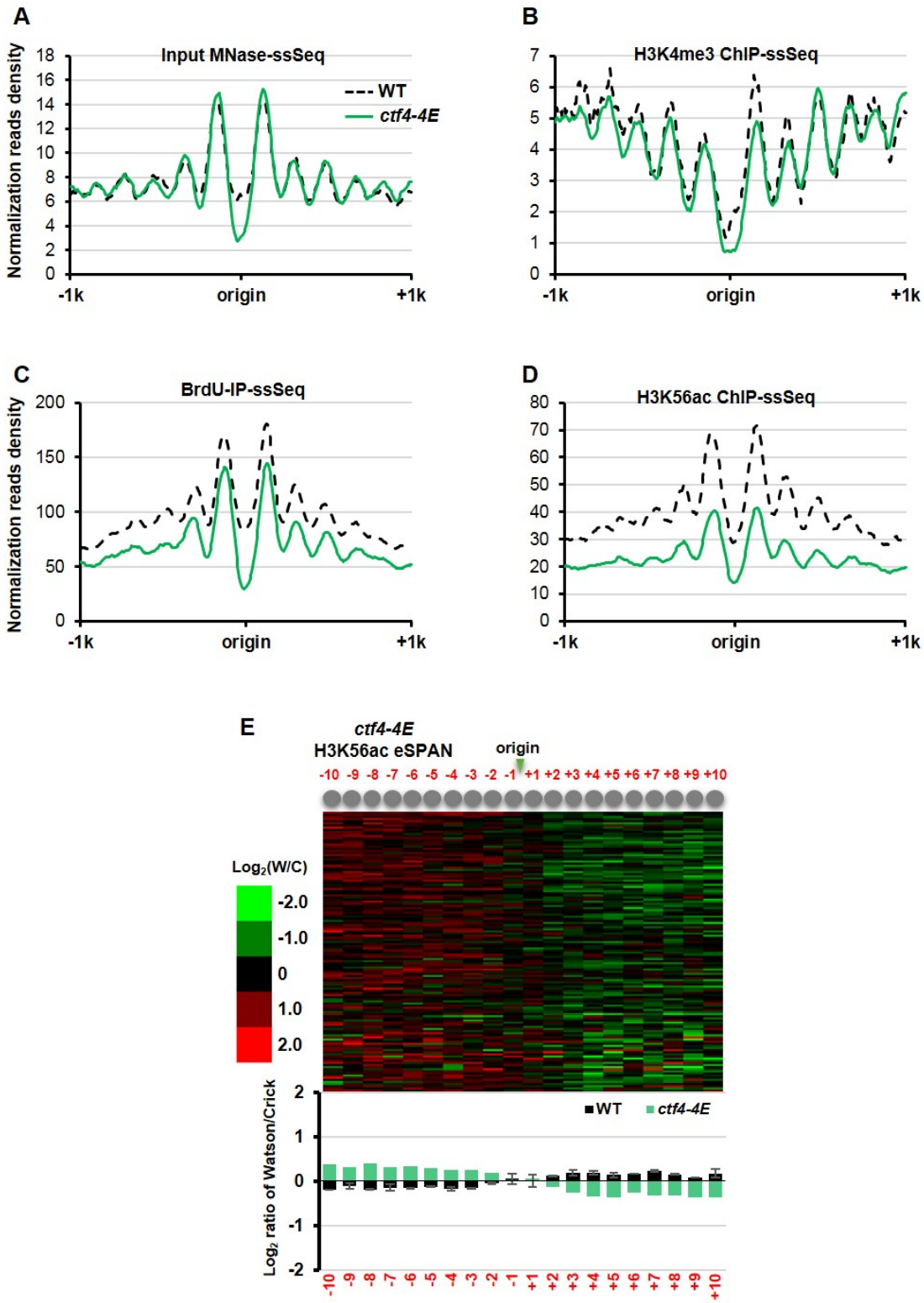
A
Input MNase-ssSeq
WT
ctf4-4E
Normalization reads density
-1k
origin
+1k
B
H3K4me3 ChIP-ssSeq
C
BrdU-IP-ssSeq
D
H3K56ac ChIP-ssSeq
E
ctf4-4E
H3K56ac eSPAN
origin
Log2(W/C)
-2.0
-1.0
0
1.0
2.0
WT
ctf4-4E
Log2 ratio of Watson/Crick

Figure S5. Nucleosome occupancy in *ctf4-4E* cells as detected by MNas-ssSeq and H3K4me3 ChIP-ssSeq is not affected, similar to *ctf4*Δ cells. Related to Figure 6. (**A-D)** Average nucleosome profiles of MNase-ssSeq of input samples (A), H3K4me3 ChIP-ssSeq (B), BrdU-IP-ssSeq (C), and H3K56ac ChIP-ssSeq (D) surrounding 134 early replication origins in wild type and *ctf4-4E* cells. Nucleosome density was calculated following the same procedure as in Figure S1. Note: the reduced nucleosome occupancy as detected by BrdU-IP-ssSeq and H3K56ac ChIP-ssSeq is likely due to the normalization effect because the DNA replication in *ctf4-4E*, similar to that in *ctf4*Δ mutant, proceeds further (data not shown). **(E)** The H3K56ac eSPAN peaks of *ctf4-4E* shows a small lagging strand bias. Top: Heatmap representing the bias pattern in *ctf4-4E* mutant cells of H3K56ac eSPAN peaks at each of the 20 individual nucleosomes surrounding 134 early DNA replication origins. The origins were ranked from top to bottom based on the replication efficiency. Bottom: the average bias ratio of H3K56ac eSPAN peaks in wild type and *ctf4-4E* mutant cells at each of the 20 individual nucleosomes of the 134 early replication origins.

Figure S6

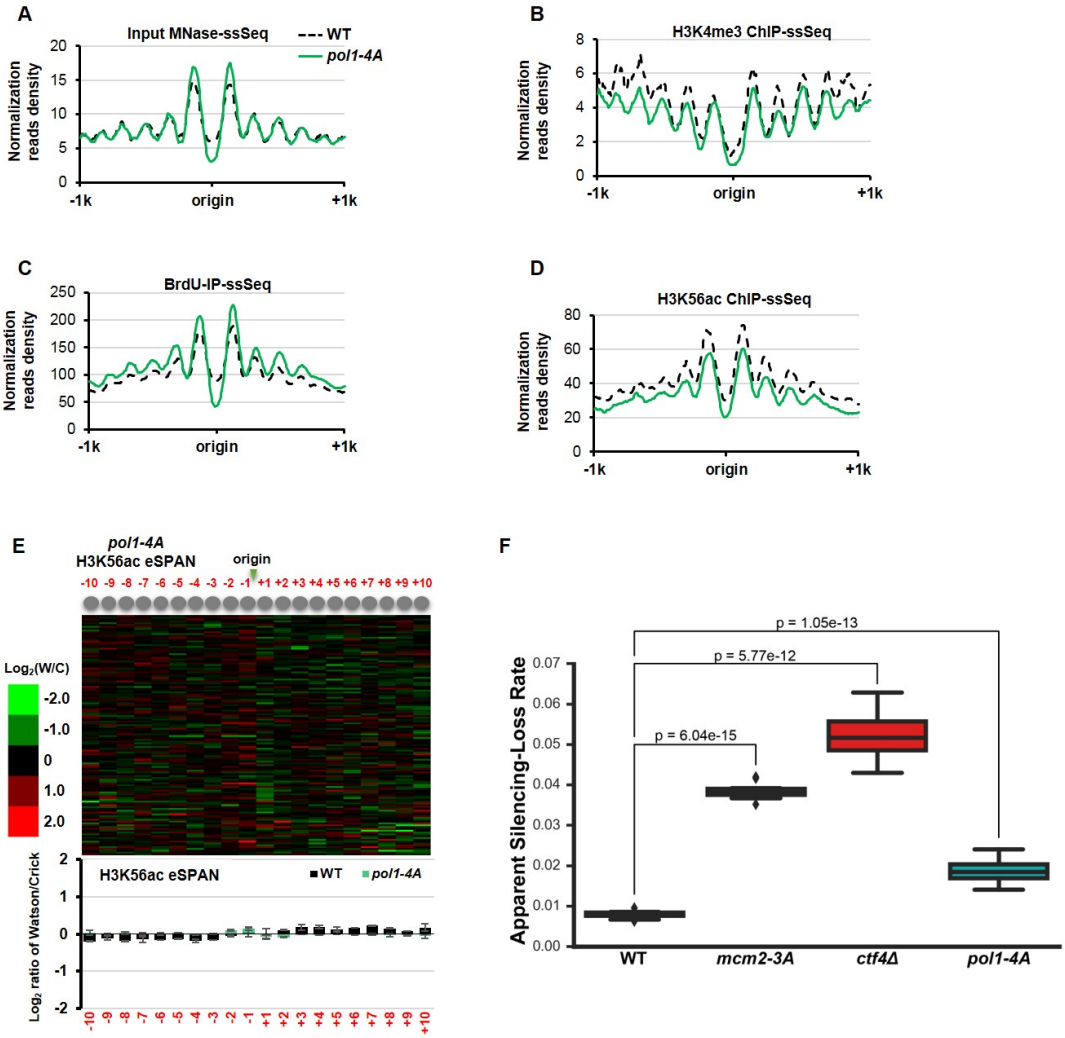

Figure S6. Cells with *mcm2-3A*, *ctf4Δ*, or *pol1-4A* mutation display an increased loss of silencing at the *HML* locus. Related to Figure 6. (A-D) The *pol1-4A* mutation has little impact on overall nucleosome occupancy and positioning surrounding early DNA replication origins. Average nucleosome profiles of MNase-ssSeq of input samples (A), H3K4me3 ChIP-ssSeq (B), BrdU-IP-ssSeq (C), and H3K56ac ChIP-ssSeq (D) surrounding 134 early replication origins in wild type and *pol1-4A* cells. Nucleosome density was calculated following the same procedure as in Figure S1. **(E)** H3K56ac eSPAN of *pol1-4A* cells show no bias towards either leading or lagging strands. Top: heatmap representing the bias pattern in *pol1-4A* mutant cells of H3K56ac eSPAN peaks

at each of the 20 individual nucleosomes surrounding 134 early DNA replication origins ranked from top to bottom based on the replication efficiency. Bottom panel: The average bias ratio of H3K56ac eSPAN peaks in wild type and *pol1-4A* mutant cells at each of the 20 individual nucleosomes of the 134 early replication origins. **(F)** Cells with *mcm2-3A*, *ctf4Δ*, or *pol1-4A* mutation display an increased loss of silencing at the *HML* locus compared to wild type cells. p values were calculated using a Welch's t-test.

Table S1: Yeast strains used in this study

Strain	Genotype	Reference
CYC560	*MATA ade2-1 ura3-1 his3-11,15 trp1-1 leu2-3,112 can1-100 URA3::BrdU–Inc*	(Yu et al., 2018)
ZGY2565	*MATA ade2-1 ura3-1 his3-11,15 trp1-1 leu2-3,112 can1-100 bar1::hisG POL1-5flag::kanMX6+ URA3::BrdU–Inc*	(Yu et al., 2014)
CYC126	*MATA ade2-1 ura3-1 his3-11,15 trp1-1 leu2-3,112 can1-100 MCM6-3HA::LEU +URA3::BrdU–Inc*	(Yu et al., 2014)
CYC511	*MATA ade2-1 ura3-1 his3-11,15 trp1-1 leu2-3,112 can1-100 mcm2-3A::hphNT LEU2::BrdU–Inc*	This study
CYC662	*MATA his3Δ200 leu2Δ0 lys2Δ0 met15Δ0 ura3Δ0 Δhhf1-hht1::LEU2 HIS3::Ptdh3_CRE_EBD78 hht2::HHT2-LoxP-HA-HYG-LoxP-T7 mcm2-3A::KanMX+ URA3::BrdU–Inc*	This study
ASC044	*MATA ade2-1 ura3-1 his3-11,15 trp1-1 leu2-3,112 can1-100 ctf4-4E URA3::BrdU–Inc*	This study
ASC049	*MATA ade2-1 ura3-1 his3-11,15 trp1-1 leu2-3,112 can1-100 pol1-4A::hphNT URA3::BrdU–Inc*	This study
ASC050	*MATA ade2-1 ura3-1 his3-11,15 trp1-1 leu2-3,112 can1-100 ctf4Δ::kanMX URA3::BrdU–Inc*	This study
JRY9628	*matΔ::natMX lys2 his3-11,15 leu2-3,112 can1-100 hml::cre ura3Δ::GPDpro-loxP-yEmRFP-CYC1term-kanMX-loxP-yEGFP-ADH1term*	(Dodson and Rine, 2015)
ASC118	*matΔ::natMX lys2 his3-11,15 leu2-3,112 can1-100 hml::cre ura3Δ::GPDpro-loxP-yEmRFP-CYC1term-kanMX-loxP-yEGFP-ADH1term mcm2-3A*	This study
ASC127	*matΔ::natMX lys2 his3-11,15 leu2-3,112 can1-100 hml::cre ura3Δ::GPDpro-loxP-yEmRFP-CYC1term-kanMX-loxP-yEGFP-ADH1term ctf4Δ::kanMX*	This study
ASC131	*matΔ::natMX lys2 his3-11,15 leu2-3,112 can1-100 hml::cre ura3Δ::GPDpro-loxP-yEmRFP-CYC1term-kanMX-loxP-yEGFP-ADH1term pol1-4A*	This study

Table S2: Primers used in this study for CRISPR/Cas9 mutagenesis

Primer	Sequence
mcm2-3A_sgRNA_5	gatcTAATATGTATGACGATTATGgttttagagctag
mcm2-3A_sgRNA_3	ctagctctaaaacCATAATCGTCATACATATTA
mcm2-3A_repair_Fw	AACGAAGTAGATTTGATGGACGATAATATGGCTGA CGATGCAGCAGCTGATCATAATAGA
mcm2-3A_repair_Rv	TTGTTCCCTGTCGTCAACTTGATCTGGATCAGCTCT ATCTCTATTATGATCAGCTGCTGC
pol1-4A_sgRNA_5	gatcGATAATTTTGATGACATTCTgttttagagctag
pol1-4A_sgRNA_3	ctagctctaaaacAGAATGTCATCAAAATTATC
pol1-4A_repair_Fw	GCAAAAAAATCCCAAAAAAAAAGTATCCCCATCGA TAATTTTGCTGCCATTGCTGGTGAG
pol1-4A_repair_Rv	GCAGTAAAATATTGGGTTTTTCTACTTCACCAGATT CAGCCTCACCAGCAATGGCAGCAA